Research Article Vol. 59, No. 9 / 20 March 2020 / Applied Optics 2695

applied optics

Mid-wave and long-wave infrared dual-band stacked metamaterial absorber for broadband with high refractive index sensitivity

Enzhu Hou,[1,2] Dejia Meng,[1] Zhongzhu Liang,[1,*] Ying Xiong,[1,2] Fuming Yang,[1,2] Yinhui Tang,[1,2] Yandong Fan,[1,2] Zheng Qin,[1,2] Xiaoyan Shi,[1,2] Yuhao Zhang,[1,2] Jingqiu Liang,[1] Changhong Chen,[3] and Jianjun Lai[3]

[1]State Key Laboratory of Applied Optics, Changchun Institute of Optics, Fine Mechanics and Physics, Chinese Academy of Sciences, Changchun, Jilin 130033, China
[2]University of the Chinese Academy of Sciences, China
[3]Wuhan National Laboratory for Optoelectronics, Huazhong University of Science and Technology, Wuhan 430074, China
*Corresponding author: liangzz@ciomp.ac.cn

Received 21 November 2019; revised 16 February 2020; accepted 16 February 2020; posted 19 February 2020 (Doc. ID 384027); published 12 March 2020

A dual-band metamaterial absorber based on local surface plasmon resonance is designed, which is composed of a periodic arrangement of stacked nanodisk structures. The structure unit consists of two dielectric layers and three metal layers. Based on the finite difference time domain method, under the condition of vertically incident plane light, two absorption peaks in the mid-wave infrared and long-wave infrared (MWIR/LWIR) are obtained, and the absorption is greater than 98%. The absorber has good incident state tolerance characteristics. We can modulate the MWIR/LWIR absorption peaks by changing the radius of the stacked disk structure, and MWIR and LWIR dual-band broadband absorption can be achieved by integrating different size elements in the plane. The average absorption is 71% for MWIR with 1.1 μm bandwidth from 3.2 to 4.3 μm and 88% for LWIR with 3 μm bandwidth from 8.5 to 11.5 μm. At the same time, the structure also has effective refractive index (RI) sensitivity characteristics. In the RI range of 1.8–2, the maximum RI sensitivity of the LWIR and the MWIR is 1085 nm/refractive index unit (RIU) and 1472 nm/RIU, respectively.

https://doi.org/10.1364/AO.384027

1. INTRODUCTION

Research on infrared technology is receiving increasing attention because of its diverse applications in thermal infrared detection [1], thermal transmitters [2–4], infrared imaging [5,6], sensing [7,8] and other areas. Its working principle is based on different target and background radiances, and different temperature targets have different radiation characteristics to obtain target information. In the atmospheric environment, the thermal radiation of the target object can be effectively transmitted in two window bands of mid-wave infrared and long-wave infrared (MWIR/LWIR). In some specific applications, single-band (8–14 μm) detection usually has the disadvantages of lack of imaging information and susceptibility to external information interference, and it is easier to introduce false alarms. However, the detector working in both bands of the MWIR (3–5 μm) and LWIR (8–14 μm) can fully obtain useful thermal information and can effectively identify the target object from a large number of images [9,10]. For example, in the fields of security and fire detection, dual-band detectors detect more information than single-band detectors. The dual-band detectors can improve the ability to determine the authenticity of the target, suppress background information, and thereby reduce the false alarm rate. The traditional uncooled infrared detector is focused on the response of the LWIR band, and its light-absorbing material can only respond to a single LWIR range. However, the emergence of metamaterial absorbers has expanded the spectral response range of the light-absorbing material. Therefore, it can be integrated on the uncooled infrared detector to detect the wide-spectrum range of dual bands in the MWIR/LWIR region.

Metamaterial absorber is an artificially constructed composite structure with an emphasis on control characteristics. Compared with traditional absorbing media, it has the advantages of thin thickness, strong absorption capacity, controllable frequency band, and design of electromagnetic parameters of materials. Researchers carried out relevant research from the microwave [11], terahertz [12–15], and LWIR or MWIR band [16] to the visible near-infrared band [17,18], including the

study of multi-band absorbers [19,20]. Feng *et al*. designed and experimentally studied a dual-band ideal absorber based on an asymmetric T-type plasma array and obtained two different absorption peaks based on the local surface plasmon polariton (LSPP) mode [21]. Zhang *et al.* designed a symmetrically arranged elliptical structure to realize a dual-band polarization-independent absorber, and translation of the absorption peak position could be obtained by modulating the long and short axes [22]. Similarly, multi-band absorbers can be realized by integrating diverse size absorbers [2,23,24] or using mutual compensation between different structural units [13,20,25,26] in the same plane. In recent years, the use of geometric deep learning technology to design micro-nano structures to achieve specific functions is also worthy of attention [27,28]. However, for the research of infrared metamaterial absorbers, most of them are on single MWIR or LWIR absorbers, whereas less attention is paid to both MWIR (3–5 μm) and LWIR (8–14 μm) with broadband and high absorption. Compared with a single MWIR or LWIR absorber, the dual-band absorption of the MWIR/LWIR has the advantage of being able to image both high-temperature and normal-temperature targets at the same time, and it can be better applied to acquiring information about thermal infrared objects. Compared with single-band absorption, it has the characteristics of strong anti-interference ability and improved system detection and identification ability.

The common methods for achieving dual-band absorption with narrow absorption bandwidth include planar integration [8,20], stacked metal–insulator–metal (MIM) [14], and multi-mode dipole resonance [19]. However, these methods have certain limitations in the realization capability of dual band in the MWIR and LWIR bands and the broad band range of the dual bands. In this paper, to reduce the planar integration method caused by impedance matching, where it is difficult to achieve the limitation of large absorption peak interval and high absorption [2], a stacked structure is designed. Different from the common stacked structure, all of the constituent layers are patterned, except for the base reflective layer, and accompanied by the design of different pattern radius. The compensation for high-order resonance is realized, and the flexibility for broadband absorption is improved. In applications, dual-band infrared absorption in the MWIR/LWIR region is better than a single MWIR or LWIR absorber, because it can simultaneously image high-temperature and room-temperature targets and improve the ability to determine the authenticity of the target, suppress background information, and reduce false alarm rates.

In this work, we design a metamaterial absorber with a double metal–dielectric–metal (MDM) structure based on the local surface plasmon (LSP) dipole resonance, which can achieve a high absorption in the MWIR/LWIR bands at the same time. Due to the different dielectrics in the MDM structure and the corresponding electromagnetic response, the stacked structure composed of Ge with a larger relative permittivity and SiO_2 with a smaller relative permittivity is designed to realize a high LWIR and MWIR absorption. The absorption response to the LWIR light is realized by Au-Ge, and the MWIR absorption is related to Au-SiO_2 and Au-Ge. In addition, our results also demonstrate that the absorber has better dimensional adjustment characteristics and incident angle stability. Dual-band broadband absorption of MWIR/LWIR can be realized by the planar combination of the primitive structures. At the same time, the absorber can realize dual-band high refractive index (RI) sensitivity for the MWIR and LWIR peaks.

2. STRUCTURE DESIGN

Figure 1 depicts the characteristic unit cell structure of the periodic nanoarray. Built on the physical mechanism of the LSP resonance of the MDM structure [29], dual-band MWIR/LWIR absorption is realized by the stacked disc structure. Figure 1(c) shows the structure we designed. There are five functional layers, and the three metal layers are separated by two dielectric layers. To reach different absorption bands, we chose SiO_2 with a relatively low dielectric constant and Ge with a relatively high dielectric constant. The two materials are used as the intermediate layer of the MDM structure, i.e., two MDM structures are formed. Here, Au is chosen as the metal. All parameters including the complex RI are derived from the results of Palik's experimental test [30]. By setting the thickness of the intermediate metal layer to greater than the skin depth, the electromagnetic characteristics of the upper and lower MDM structures have no impact.

We performed a numerical analysis based on the finite difference time domain (FDTD) method to study the electromagnetic properties and absorption of the resonant unit (where A is the absorption, R is the reflectance, and T is the transmittance). The feature sizes of the absorbers are shown in Figs. 1(c) and 1(d), in which the top layer Au thickness (h_1) is 0.04 μm, and the middle layer (h_3) and bottom substrate (h_5) Au have a thickness of 0.05 μm. Because the thickness of the base metal is greater than the skin depth of the infrared region, the propagation transmittance of the structure can be approximated as 0, i.e., $T = 0$. Therefore, the absorption characteristics of the structure are determined by the frequency-dependent reflectance R. To achieve high absorption, according to the s-parameter inversion method [31,32], we need to design the impedance matching between the equivalent impedance of the metamaterial absorber [$Z(\omega)$] and the free space (Z_0). The reflectivity of a composite material can be expressed as

$$R(\omega) = \left[\frac{Z(\omega) - Z_0}{Z(\omega) + Z_0}\right]^2. \tag{1}$$

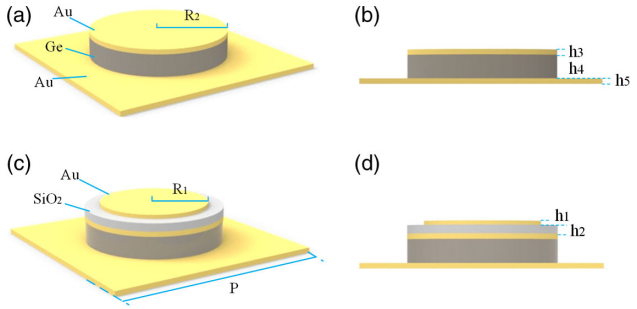

Fig. 1. Design of the infrared metamaterial absorber. (a) and (b) Structure of the Au-Ge-Au metamaterial absorber unit cell with dimensions of $h_3 = 0.05$ μm, $h_4 = 0.22$ μm, $h_5 = 0.05$ μm, and $R_2 = 0.7$ μm. (c) and (d) Stacked Au-SiO_2 dual-band metamaterial absorbers with additional dimensions of $h_1 = 0.04$ μm, $h_2 = 0.08$ μm, and $R_1 = 0.58$ μm. The period is 2.2 μm.

If we want to make the R reflectance 0, we need to make the structure achieve $Z(\omega) = Z_0$ [13]. For the MDM structure of the metamaterial absorbers, the thickness of the intermediate dielectric layer is critical because it affects the resonant intensity of the electromagnetic dipole; as the thickness increases, the resonance effect decreases, and the overall absorption efficiency decreases. By designing the thicknesses of Ge and SiO_2 and the structural radius R_1 and R_2 of the stacked structure, we obtain a high absorption of the structure of the metamaterial absorber structure. The final thicknesses of Ge and SiO_2 are 0.22 μm (h_4) and 0.08 μm (h_2), respectively.

3. RESULT AND DISCUSSION

A. Dual-Band Metamaterial Absorber

The absorption of the stacked structure [Au-Ge-Au-SiO_2-Au, AGASA, Fig. 1(c)] and the common MDM structure [Au-Ge-Au, AGA, Fig. 1(a)] are shown in Fig. 2. By comparing the results of the AGASA structure ($R_2 = 0.7$ μm, $R_1 = 0.58$ μm) and those of the AGA structure ($R_2 = 0.7$ μm), we find that the AGA structure achieves high absorption in the MWIR 3.79 μm and LWIR 9.97 μm regions, and the two absorption peaks are greater than 98%. The absorption of the AGASA structure with stacked Au-SiO_2 is almost unchanged in the LWIR region, whereas the MWIR absorption is broadened compared to the original structure, and FWHM widened from 0.17 to 0.48 μm. The reason the MWIR bandwidth broadens is to use R_1 of the top Au to achieve an absorption peak with a smaller peak interval from the higher-order resonance of Au-Ge-Au and to achieve broadening of the MWIR bandwidth under the combined action of two resonances. Additionally, the MWIR absorption peak is redshifted, moving to 3.89 μm, and this absorption includes the absorption of the AGA structure in the MWIR region. It is clearly shown that the MWIR absorption of the AGA structure is narrower and sharper, and there are some limitations in practical applications. However, smoothing and broadening of the spectral line is achieved by the coupling compensation of the AGASA structure with stacked Au-SiO_2.

To understand the absorption mechanism of the stacked structure, we calculated and analyzed the electromagnetic field distribution of the structure. As shown in Figs. 3(a) and 3(d), in

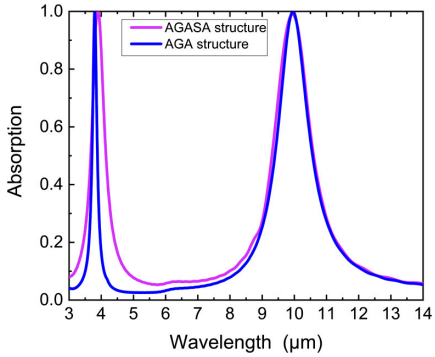

Fig. 2. Calculated time domain absorption spectrum of the designed dual-band metamaterial absorber. Absorption spectrum of the AGA structure (purple curve) and absorption spectrum of the AGASA structure with the stacked Au-SiO_2 (red curve) in the wavelength range from 3–14 μm.

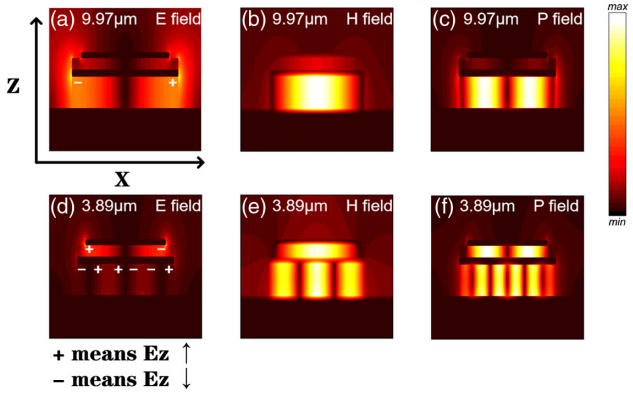

Fig. 3. Cross-sectional views of the electromagnetic field and energy distributions in the proposed structure corresponding to the normal spectral absorption peaks: the (a) electric field, (b) magnetic field, and (c) energy distributions for the LWIR absorption peak at 9.97 μm, and the (d) electric field, n magnetic field, and (f) energy density distributions for the MWIR absorption peak at 3.89 μm.

the absorber structure, electric dipole coupling occurs at the resonant wavelength, and the electric field is limited at the interface edge of the upper metal to the dielectric. The LWIR absorption is realized by the LSP eigenmode dipole resonance of the Au-Ge interface, and the MWIR absorption is realized by the LSP eigenmode dipole resonance of the Au-SiO_2 interface and the LSP high-order dipole resonance of the Au-Ge interface [26]. At the same time, we get the z-axis component of the electric field from the figure. Under the action of the reverse electric field, the movement of free electrons can be equivalent to a circulating current formed between the two metal layers and generating a magnetic moment that strongly interacts with the incident optical magnetic field [6,33] such that the magnetic field is restricted to the media. Therefore, at the resonant frequency, the local electromagnetic field between the two metal layers is strongly enhanced, and the incident electromagnetic energy can be effectively confined in the intermediate dielectric spacer layer, which can be obtained from the energy density distribution of Figs. 3(e) and 3(f). This energy is then converted to thermal energy by loss, resulting in a nearly zero reflectance.

In summary, the absorption at 9.97 μm is mainly achieved by the LSP eigenmode dipole resonance of the Au-Ge structure, and the absorption at 3.89 μm is achieved by the LSP of the eigenmode dipole resonance of Au-SiO_2 and the high-order dipole resonance of Au-Ge. It can also be explained that in the absence of stacking, the MWIR absorption at 3.75 μm is due to the high-order electric dipole resonance.

B. Energy Loss

The electromagnetic energy coupled in the dielectric layer will eventually be absorbed by the components of the stacked absorber in the form of thermal energy. The energy absorption curve of the components is shown in the Fig. 4. It is shown that the electromagnetic energy coupled in the dielectric layer is mostly absorbed by the Au layer in the form of ohmic losses, rather than absorbed by Ge and SiO_2 in the form of dielectric losses. This is because metal materials have a higher imaginary part of the RI, which is the main factor affecting the absorption

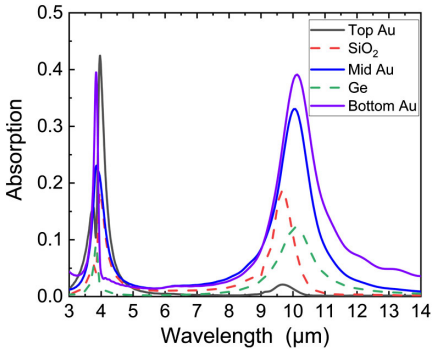

Fig. 4. Energy absorption of each layer of the stacked structure.

capacity of the material. And it is shown from the curve that the top Au mainly absorbs the MWIR spectral energy of the Au-SiO_2 coupled electromagnetic field, with less of the spectral energy of the Au-Ge coupled electromagnetic field, the bottom Au absorbs Au-Ge coupled to the spectral energy of the electromagnetic field, and the middle Au absorbs both coupled spectral energy.

C. Incident Angle Stability

The angle dependence of the performance of our dual-band metamaterial absorber is further studied. Figures 5(a) and 5(b) show the absorption behavior of the structure at different incident angles for TM and TE polarization states, respectively. First, the absorption mechanism of the dual-band absorber we designed is based on LSP resonance. Its absorption peak is mainly determined by the structure size and material, regardless of the angle of incidence. Then, the stability of the structure relative to the incident angle mainly depends on the thickness of the micro-nano periodic array unit cell. The smaller the thickness is, the better the angular stability, and the less likely the performance changes with the changing of the incident angle. Because the metal selected for the structural design is Au, the thickness of the dielectric required for the metal to achieve impedance matching is much smaller than Ti, Ni, etc. It is shown that the absorption condition is relatively stable when the incident angle is less than $\pm 45^{\circ}$, indicating that the absorber has good incident state tolerance characteristics.

D. Size Modulation and Bandwidth Expansion

The physical mechanism of strong absorption is mainly due to the electric dipole resonance caused by the LSP at the junction

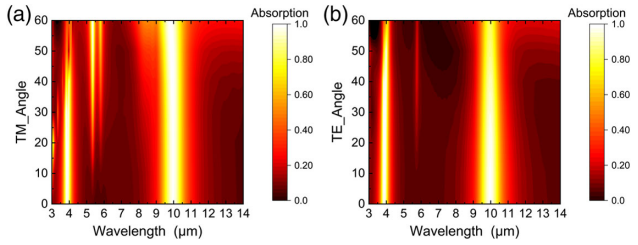

Fig. 5. Absorption contour maps of the absorber as a function of incident angle and wavelength under oblique incident angles from 0° to 60° with a step size of 10°. (a) TM and (b) TE polarization states.

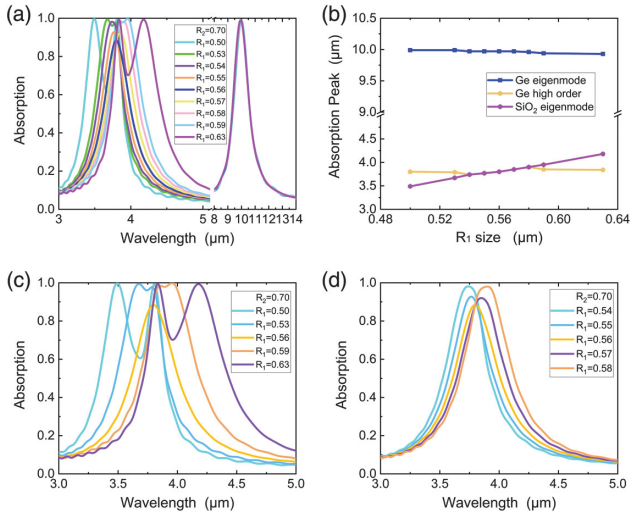

Fig. 6. (a) Absorption of stacked structures with different R_1, (b) corresponding changes in absorption peaks with R_1, and (c) and (d) gradual change of absorption with R_1.

of the metal and dielectric, and the absorption can be modulated by changing the structure size. Figure 6(a) shows the variation in absorption as the feature size R_1 increases without changing the period of the stacked disk array. The variation in the absorption peak with the feature size R_1 ranging from 0.5 to 0.63 μm is illustrated in Fig. 6(b). The LWIR absorption is hardly changed, whereas the number of the MWIR absorption peaks changes from two to one and finally to two. In Fig. 6(c), R1 is taken as 0.50, 0.53, 0.56, 0.59, and 0.63 (μm) to depict redshift of the absorption peak generated by the eigenmode dipole resonance of Au-SiO_2 with the increase of R_1. The Au-Ge high-order resonance absorption peak completely coincides with the Au-SiO_2 eigenmode dipole resonance absorption peak at R_1 of 0.56 μm. Figure 6(d) shows the MWIR absorption peak of when R_1 is 0.54, 0.55, 0.56, 0.57, and 0.58 (μm), and there is only one absorption peak. Due to the differences in R_1, the two kinds of resonance coupling compensation are not the same, and the high-order absorption peak does not completely coincide with the position of the Au-SiO_2 absorption peak, i.e., 0.56 μm.

The structural characteristics of our dual-band absorber were further studied by changing the radius R_1 and R_2 of the stacked disks. Figure 6 depicts that by modulating R_1 and R_2, we achieve double absorption peak modulation for the MWIR/LWIR peaks, with R_2 being 0.65, 0.7, 0.75, and 0.8 (μm), corresponding to R_1 being 0.54, 0.58, 0.63, and 0.68 (μm), respectively. The increase in the radius of the nanodisk causes a redshift of the absorption peak, which is due to the redshift of the plasmon resonance in each particle increasing as the size of the structural features increases. When R_2 corresponds to dual-band absorption at 0.8 μm, another absorption peak with a lower absorption appears in the LWIR region, because the increase in R_1 to match R_2 causes the surface Au-SiO_2 structure to produce this absorption under this condition.

Through the planar integration method, four different sizes of the stacked structures were combined to widen the MWIR/LWIR absorption bandwidth. According to the structural modulation characteristics of the absorber, R_2 (0.83, 0.78,

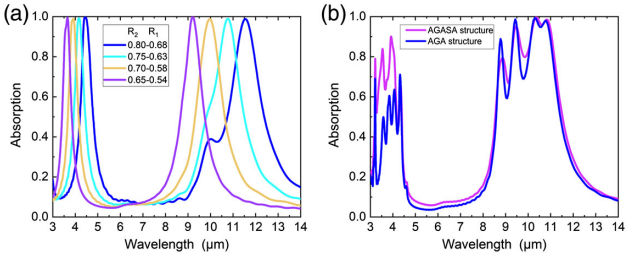

Fig. 7. (a) Coordination of R_1 and R_2 to achieve adjustment of MWIR/LWIR dual-band absorption peaks. (b) Combination of four different sizes of the stacked disk structure to achieve MWIR/LWIR absorption bandwidth expansion.

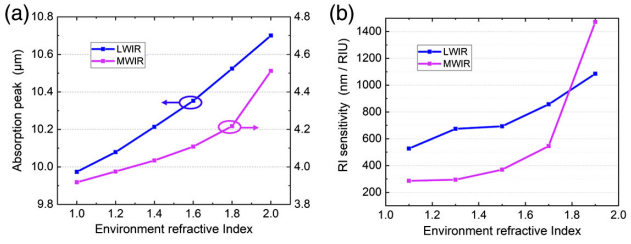

Fig. 8. (a) Absorber absorption peak position changes with environmental RI. (b) Calculated RI sensitivity (purple depicts the MWIR peak and blue depicts the LWIR peak).

0.73, 0.68 μm) and R_1 (0.6, 0.57, 0.54, 0.51 μm) are modulated to achieve compensation and broadband absorption in the MWIR/LWIR band. To reduce the absorption reduction phenomenon due to the increase in the period of the combined structure, the dielectric loss is enhanced by increasing the thicknesses of Ge and SiO_2 to 0.46 μm (h_4) and 0.13 μm (h_2), respectively. Figure 7 depicts the combination of four different size stacked structures achieving a maximum absorption peak of 90%, the half-wave width of 1.76 μm, and an average absorption (3.2–4.3 μm) of 71% in the MWIR region; the maximum absorption peak is 99%, the half-wave width is 3.2 μm, and the average absorption (8.5–11.5 μm) is 88% in the LWIR region. It can be understood from the comparison in the figure and the above calculation that the AGASA composite structure has a higher broadband absorption than the AGA combined structure, which occurs because the Au-SiO_2 structure compensation method is used to improve the MWIR absorption efficiency. The change in the LWIR absorption is due to the effect of the LWIR dipole resonance of the stacked Au-SiO_2 with larger R_1, so the absorption in the gap is enhanced for each absorption peak.

E. Environmental RI Sensitivity

To study the potential of our designed metamaterial absorber based on the stacked disk structure as a RI sensor, we simulated the effect of different RI environments on the absorption of the structure, in which the RI was increased from 1 to 2, as shown in Fig. 8. When the ambient RI increases from 1 to 2, the structure we designed can always exhibit two absorption peaks in the MWIR and LWIR ranges, but increasing the environmental RI will result in a small decrease in the absorption. The RI sensitivity S_{RI} used to evaluate the RI sensitivity is defined as the dependence of the absorption peak position changes on the RI [29]:

$$S_{RI} = \frac{\Delta\lambda_{res}}{\Delta n}. \quad (2)$$

The dual-band RI sensitivity was analyzed by the linear regression method of least squares. Figure 8 shows the effect of the ambient RI changing from 1 to 2 on the absorption peak positions of the stacked structure and the RI sensitivity. Figure 8(a) shows the relationship between the RI and the positions of the absorption peaks. As the RI increases, the MWIR/LWIR absorption peaks are redshifted. The RI sensitivity is defined as the slope of the linear regression. Through calculation, the RI sensitivity of the LWIR peak is 731 nm/refractive index unit (RIU), and the RI sensitivity of the MWIR coupling mode is 538 nm/RIU. However, we can see in Fig. 8(a) that the RI sensitivity is not completely linear with the change in the RI from 1 to 2. By calculation, we can see from Fig. 8(b) that as the RI increases, the RI sensitivity also becomes larger. In the RI range of 1.8–2, the LWIR maximum RI sensitivity is 1085 nm/RIU, and the MWIR maximum RI sensitivity is 1472 nm/RIU. Referring to recent research on the RI sensing of absorbers [8,34–36], it is shown that the structure has effective RI sensitivity, which indicates its potential application in RI sensors. The dual-band sensing features a wide range of results for calibration and application in the MWIR and LWIR. Ordinary RI sensor devices generally have the following characteristics: low loss and high RI sensitivity and quality factor, which are all characteristics that can be optimized in the structure for use as a sensor in the future.

4. SUMMARY

A dual-band metamaterial absorber in the MWIR/LWIR regime is achieved by utilizing a stacked double-MDM nanostructure. The absorption at the mid-wave of 3.89 μm and long-wave 9.97 μm is about 99% with the device maintaining high absorption at incident angles up to ±45°. The adjustment of the array structure unit sizes R_1 and R_2 can realize the modulation of the MWIR/LWIR resonance peak positions. The designed plane integrating four different sizes of the stacked structure achieves, in the MWIR range, a maximum absorption peak of 90%, a half-wave width of 1.76 μm, and an average absorption of 71% from 3.2 to 4.3 μm, and in the LWIR range, a maximum absorption peak of 99%, a half-wave width of 3.2 μm, and an average absorption of 88% in the range of 8.5 to 11.5 μm. The metamaterial absorber has a high RI sensitivity, and as the RI increases, the RI sensitivity increases. The absorber has great potential for RI sensing applications through comparative analysis.

Funding. National Natural Science Foundation of China (61735018, 61376122, 61805242); Scientific and Technological Development Project of Jilin Province (20170204077GX, 20190103014JH); Excellent Member of Youth Innovation Promotion Association CAS (2014193); Leading Talents and Team Project of Scientific and

Technological Innovation for Young and Middle-Aged Groups in Jilin Province (20190101012JH); Overseas Students Science and Technology Innovation and Entrepreneurship Projects; Project of CIOMP-Duke Collaborative Research (201903002); Project of CIOMP-Fudan University Collaborative Research; Independent fund of State Kay Laboratory of Applied Optics.

Disclosures. The authors declare no conflicts of interest.

REFERENCES

1. J. J. Talghader, A. S. Gawarikar, and R. P. Shea, "Spectral selectivity in infrared thermal detection," Light Sci. Appl. **1**, e24 (2012).
2. X. Liu, T. Tyler, T. Starr, A. F. Starr, N. M. Jokerst, and W. J. Padilla, "Taming the blackbody with infrared metamaterials as selective thermal emitters," Phys. Rev. Lett. **107**, 045901 (2011).
3. K. Du, L. Cai, H. Luo, Y. Lu, J. Tian, Y. Qu, P. Ghosh, Y. Lyu, Z. Cheng, M. Qiu, and Q. Li, "Wavelength-tunable mid-infrared thermal emitters with a non-volatile phase changing material," Nanoscale **10**, 4415–4420 (2018).
4. C. F. Doiron and G. V. Naik, "Non-Hermitian selective thermal emitters using metal-semiconductor hybrid resonators," Adv. Mater. **31**, 1904154 (2019).
5. A. Tittl, A. K. Michel, M. Schaferling, X. Yin, B. Gholipour, L. Cui, M. Wuttig, T. Taubner, F. Neubrech, and H. Giessen, "A switchable mid-infrared plasmonic perfect absorber with multispectral thermal imaging capability," Adv. Mater. **27**, 4597–4603 (2015).
6. R. Feng, J. Qiu, Y. Cao, L. Liu, W. Ding, and L. Chen, "Wide-angle and polarization independent perfect absorber based on one-dimensional fabrication-tolerant stacked array," Opt. Express **23**, 21023–21031 (2015).
7. H. Huang, H. Xia, W. Xie, Z. Guo, H. Li, and D. Xie, "Design of broadband graphene-metamaterial absorbers for permittivity sensing at mid-infrared regions," Sci. Rep. **8**, 4183 (2018).
8. J. Xu, Z. Zhao, H. Yu, L. Yang, P. Gou, J. Cao, Y. Zou, J. Qian, T. Shi, Q. Ren, and Z. An, "Design of triple-band metamaterial absorbers with refractive index sensitivity at infrared frequencies," Opt. Express **24**, 25742–25751 (2016).
9. A. Ishikawa and T. Tanaka, "Metamaterial absorbers for infrared detection of molecular self-assembled monolayers," Sci. Rep. **5**, 12570 (2015).
10. P. Yu, J. Wu, E. Ashalley, A. Govorov, and Z. Wang, "Dual-band absorber for multispectral plasmon-enhanced infrared photodetection," J. Phys. D **49**, 365101 (2016).
11. F. Ding, Y. Cui, X. Ge, Y. Jin, and S. He, "Ultra-broadband microwave metamaterial absorber," Appl. Phys. Lett. **100**, 103506 (2012).
12. Y. Ma, Q. Chen, J. Grant, S. C. Saha, A. Khalid, and D. R. Cumming, "A terahertz polarization insensitive dual band metamaterial absorber," Opt. Lett. **36**, 945–947 (2011).
13. M. Kenney, J. Grant, Y. D. Shah, I. Escorcia-Carranza, M. Humphreys, and D. R. S. Cumming, "Octave-spanning broadband absorption of terahertz light using metasurface fractal-cross absorbers," ACS Photon. **4**, 2604–2612 (2017).
14. B. X. Wang, G. Z. Wang, T. Sang, and L. L. Wang, "Six-band terahertz metamaterial absorber based on the combination of multiple-order responses of metallic patches in a dual-layer stacked resonance structure," Sci. Rep. **7**, 41373 (2017).
15. H. R. Seren, J. Zhang, G. R. Keiser, S. J. Maddox, X. Zhao, K. Fan, S. R. Bank, X. Zhang, and R. D. Averitt, "Nonlinear terahertz devices utilizing semiconducting plasmonic metamaterials," Light Sci. Appl. **5**, e16078 (2016).
16. Y. Li, B. An, L. Li, and J. Gao, "Broadband LWIR and MWIR absorber by trapezoid multilayered grating and SiO_2 hybrid structures," Opt. Quantum Electron. **50**, 459 (2018).
17. N. Liu, M. Mesch, T. Weiss, M. Hentschel, and H. Giessen, "Infrared perfect absorber and its application as plasmonic sensor," Nano Lett. **10**, 2342–2348 (2010).
18. F. Ding, J. Dai, Y. Chen, J. Zhu, Y. Jin, and S. I. Bozhevolnyi, "Broadband near-infrared metamaterial absorbers utilizing highly lossy metals," Sci. Rep. **6**, 39445 (2016).
19. Z. Liu, G. Liu, G. Fu, X. Liu, and Y. Wang, "Multi-band light perfect absorption by a metal layer-coupled dielectric metamaterial," Opt. Express **24**, 5020–5025 (2016).
20. B. Mulla and C. Sabah, "Multiband metamaterial absorber design based on plasmonic resonances for solar energy harvesting," Plasmonics **11**, 1313–1321 (2016).
21. R. Feng, W. Ding, L. Liu, L. Chen, J. Qiu, and G. Chen, "Dual-band infrared perfect absorber based on asymmetric T-shaped plasmonic array," Opt. Express **22**, A335–A343 (2014).
22. B. Zhang, Y. Zhao, Q. Hao, B. Kiraly, I. C. Khoo, S. Chen, and T. J. Huang, "Polarization-independent dual-band infrared perfect absorber based on a metal-dielectric-metal elliptical nanodisk array," Opt. Express **19**, 15221–15228 (2011).
23. C. Liu, L. Qi, and M. Wu, "Triple-broadband infrared metamaterial absorber with polarization-independent and wide-angle absorption," Opt. Mater. Express **8**, 2439–2448 (2018).
24. L. Zhao, H. Liu, Z. He, and S. Dong, "Theoretical design of twelve-band infrared metamaterial perfect absorber by combining the dipole, quadrupole, and octopole plasmon resonance modes of four different ring-strip resonators," Opt. Express **26**, 12838–12851 (2018).
25. W. Ma, Y. Wen, and X. Yu, "Theoretical and experimental demonstrations of a dual-band metamaterial absorber at mid-infrared," IEEE Photon. Technol. Lett. **26**, 1940–1943 (2014).
26. Q. Mao, C. Feng, and Y. Yang, "Design of tunable multi-band metamaterial perfect absorbers based on magnetic polaritons," Plasmonics **14**, 389–396 (2018).
27. Y. Kiarashinejad, M. Zandehshahvar, S. Abdollahramezani, O. Hemmatyar, R. Pourabolghasem, and A. Adibi, "Knowledge discovery in nanophotonics using geometric deep learning," Adv. Intell. Syst. **2**, 1900132 (2019).
28. Y. Kiarashinejad, S. Abdollahramezani, and A. J. Adibi, "Deep learning approach based on dimensionality reduction for designing electromagnetic nanostructures," NPJ Comput. Mater. **6**, 12 (2019).
29. R. Ameling, L. Langguth, M. Hentschel, M. Mesch, P. V. Braun, and H. Giessen, "Cavity-enhanced localized plasmon resonance sensing," Appl. Phys. Lett. **97**, 253116 (2010).
30. E. Palik, ed., *Handbook of Optical Constants of Solids* (Academic, 1985).
31. X. Chen, T. M. Grzegorczyk, B. I. Wu, J. Pacheco, Jr., and J. A. Kong, "Robust method to retrieve the constitutive effective parameters of metamaterials," Phys. Rev. E **70**, 016608 (2004).
32. D. R. Smith, D. C. Vier, T. Koschny, and C. M. Soukoulis, "Electromagnetic parameter retrieval from inhomogeneous metamaterials," Phys. Rev. E **71**, 036617 (2005).
33. P. Ding, E. Liang, L. Zhang, Q. Zhou, and Y. X. Yuan, "Antisymmetric resonant mode and negative refraction in double-ring resonators under normal-to-plane incidence," Phys. Rev. E **79**, 016604 (2009).
34. F. Cheng, X. Yang, and J. Gao, "Enhancing intensity and refractive index sensing capability with infrared plasmonic perfect absorbers," Opt. Lett. **39**, 3185–3188 (2014).
35. L. Chen, Y. Liu, Z. Yu, D. Wu, R. Ma, Y. Zhang, and H. Ye, "Numerical investigations of a near-infrared plasmonic refractive index sensor with extremely high figure of merit and low loss based on the hybrid plasmonic waveguide-nanocavity system," Opt. Express **24**, 23260–23270 (2016).
36. W. Cui, Y. Liang, Q. Wang, Y. Liu, L. Li, M. Lu, Z. Zhang, J.-F. Masson, and W. Peng, "Dual-channel narrowband polarization absorber with high field enhancement and refractive index sensitivity based on a nanorod array," J. Opt. Soc. Am. B **35**, 237–243 (2018).